Enhanced strong-coupling stimulated Brillouin amplification assisted by Raman amplification

Y. Chen [1,2] C. Y. Zheng,[3,4,5] Z. J. Liu [3,4] L. H. Cao [3,4,5] and C. Z. Xiao[2,5,*]

[1]*School of Electrical and Information Engineering, Anhui University of Science and Technology, Huainan, Anhui 232001, China*

[2]*Key Laboratory for Micro-/Nano-Optoelectronic Devices of Ministry of Education, School of Physics and Electronics, Hunan University, Changsha 410082, China*

[3]*Institute of Applied Physics and Computational Mathematics, Beijing 100094, China*

[4]*HEDPS, Center for Applied Physics and Technology, Peking University, Beijing 100871, China*

[5]*Collaborative Innovation Center of IFSA (CICIFSA), Shanghai Jiao Tong University, Shanghai 200240, China*

(Received 27 September 2022; accepted 27 December 2022; published 17 January 2023)

Higher intensity of strong-coupling stimulated Brillouin scattering (SC-SBS) amplification is achieved by supplementary Raman amplification. In this scheme, a Raman pump laser first amplifies the seed pulse in the homogeneous plasma, and then a SC-SBS pump laser continues the amplification in the inhomogeneous plasma in order to suppress the spontaneous instability of pump lasers. The intensity of the seed laser gets higher and the duration of the seed laser gets shorter than that in the pure SC-SBS scheme with the same incident energy, while the energy conversion efficiency is not significantly reduced. We also found that the SC-SBS amplification is seeded by the leading pulse of Raman amplification. The results obtained from envelope coupling equations, Vlasov simulations, and two-dimensional particle-in-cell simulations agree with each other. This scheme offers a possible way to improve the SC-SBS amplification in experiments.

DOI: 10.1103/PhysRevE.107.015204

I. INTRODUCTION

Laser amplification by laser plasma instabilities is a promising and powerful way to produce a high-intensity laser pulse [1,2]. Using plasma as the gain medium avoids the damage of optical grating in the chirped-pulse amplification technique [3]. Two kinds of laser plasma instabilities are commonly applied to plasma-based amplification: stimulated Raman scattering (SRS) [4–24] and strong-coupling stimulated Brillouin scattering (SC-SBS) [25–42]. A seed laser pulse couples with a counterpropagating pump laser via a plasma wave, i.e., a Langmuir wave or an ion acoustic wave [43,44], and then the energy of the pump laser is transferred to the seed laser pulse leading to a rapid increase of the seed laser's intensity.

Linear and nonlinear stages exist in both Raman amplification and SC-SBS amplification. At the linear stage, the amplitude of the pump laser can be considered as a constant, so we only discuss the exponential growth of the seed laser and the plasma waves; at the nonlinear stage, linear growth of the seed laser is observed because of pump depletion, and the energy flows from the tail of the seed laser back to the pump laser, which results in the π pulses. This stage is also called the self-similar stage [18,31,34]. The duration of the leading pulse would be reduced in the nonlinear stage of Raman amplification, because the peak of the seed laser is superluminal. Early works have also observed this phenomenon in Raman amplification [4,10,12,45–47]. However, in the nonlinear stage of SC-SBS amplification, the reduction of the seed laser duration is slower than that in Raman amplification [31,34,35,40,48]; the pulse duration is usually hundreds of femtoseconds [30]. Amiranoff *et al.* [38] reported that the duration of the seed laser is related to the ratio of the intensities of the seed laser and the pump laser; therefore, using a seed laser with higher intensity may reduce the duration of the seed laser in SC-SBS amplification.

In this paper, we propose a scheme in which, by adding a short-distance Raman amplification ahead of the SC-SBS amplification, the pulse width of the seed laser is substantially reduced and the maximum intensity of the seed laser is increased markedly. First, the coupled envelope equations for SRS and SC-SBS are constructed, which contains five waves: SRS pump laser, SC-SBS pump laser, Langmuir wave, ion acoustic wave, and seed laser pulse. The maximum intensity of the amplified seed laser is increased about 36% with SRS amplification. The SC-SBS amplification is seeded by the leading pulse of SRS, because the structure of the seed laser after SRS amplification is similar to that in SC-SBS amplification. Then we discuss this phenomenon by phase analysis and find that a higher initial intensity of the seed laser will cause a shorter energy transfer region.

Next, for a more detailed discussion of the effects of SRS amplification, one-dimensional and fully kinetic Vlasov-Maxwell code (Vlama) [49] is used. A higher intensity of the seed laser is obtained, which agrees well with our five-wave amplification model. We also found that the optimal proportion of SRS is $L_{\mathrm{SRS}}/L_{\mathrm{total}} = 0.25$, where L_{SRS} is the SRS amplification length and L_{total} is the total amplification length. Under this condition, the maximum intensity of the seed laser is increased about 69%, and the energy transfer efficiency only decreases 3%, compared with pure SC-SBS amplification. It

*xiaocz@hnu.edu.cn

should be noticed that the total input energy of the pump laser, which includes the energy of the SRS pump laser and the SC-SBS pump laser, is the same as that of the pure SC-SBS case. At last, a two-dimensional particle-in-cell (PIC) code is used to investigate the influence of multidimensional effects. Similar to the one-dimensional cases, the intensity of the amplified seed laser also increases in our scheme. However, the filamentation of the seed laser is observed in two-dimensional simulations which may be harmful for the amplification.

This paper is structured in the following way. First, in Sec. II, we describe the envelope coupling equations of SRS and SC-SBS amplifications. Second, the five-wave amplification model is numerically solved to study our scheme in Sec. III. Third, Vlasov simulations and PIC simulations verify our five-wave simulation results in Secs. IV and V. At last, the conclusion and discussion about our scheme and the experimental guidance are shown in Sec. VI.

II. THEORETICAL ANALYSIS OF THE FIVE-WAVE AMPLIFICATION MODEL

Stimulated Raman scattering and strong-coupling stimulated Brillouin scattering are the commonly used laser plasma instabilities in pulse amplification. Pulse amplification by SRS has an advantage; the intensity growth of the seed laser in SRS amplification is faster than that in SC-SBS amplification at the early stage, because SRS usually has a higher growth rate. However, SRS amplification also has its disadvantages: (i) The energy transfer efficiency is low, because nearly half of the pump laser's energy flows to Langmuir waves; and (ii) the π pulses appear in the nonlinear stage, and they will absorb a part of the pump laser's energy.

Similarly, SC-SBS amplification has its advantages: (i) The energy transfer efficiency is higher. Most of the pump laser's energy flows to the seed laser, because the frequency of the ion acoustic waves is far less than the frequency of the pump laser; and (ii) the amplitude of the π pulse is lower than that in Raman amplification. The disadvantage of SC-SBS amplification is that the growth rate is lower than that of SRS, so it will take a longer time to enter the exponential growth stage [38].

A natural idea is to combine the advantages of SRS and SC-SBS to obtain a better laser amplification. In this paper, we propose a scheme of SC-SBS amplification assisted by SRS amplification. As shown in Fig. 1, Scheme 1 is the normal SC-SBS amplification in an inhomogeneous plasma. The green rectangle is the pump laser of SC-SBS, which injects from the left, and the Gaussian seed laser enters the plasma from the right. In the our scheme, a part of SC-SBS amplification is replaced by SRS amplification in the homogeneous plasma, and correspondingly, there exists the SRS pump laser in front of the SC-SBS pump laser. The duration of the SRS pump laser is obtained by $\tau_{\mathrm{SRS}} \approx 2L_{\mathrm{SRS}}/c$, where L_{SRS} is the length of SRS region and c is the light speed in vacuum.

It should be noticed that the SC-SBS amplification in nonuniform density has three advantages: (i) It can mitigate the influence of spontaneous SRS of the pump laser; (ii) the triangular density profile adds an effective chirp on the pump laser, which is favorable to amplification [48]; and (iii) the amplitude of the π pulse in the triangular density profile is

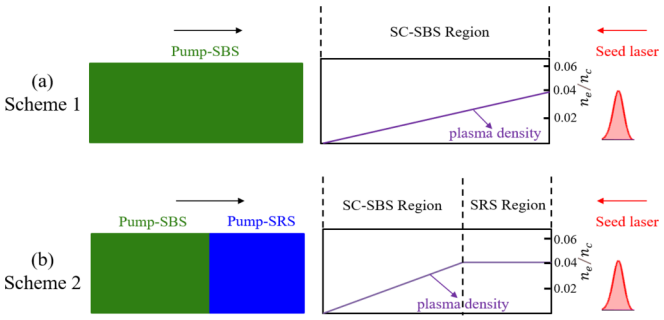

FIG. 1. (a) The pure SC-SBS amplification. (b) The five-wave amplification scheme. The plasma region is divided into the SC-SBS region and the SRS region. In front of the SC-SBS pump laser, the SRS pump laser is added.

lower than that in the uniform density profile, and the energy exchange mainly occurs at the first peak of the seed laser [38,48].

In order to describe Scheme 2, we construct five-wave envelope coupling equations including both SRS and SC-SBS [43,44]:

$$
\begin{aligned}
(\partial_t + \nu_{00} + V_{00}\partial_x)a_{00} &= -\frac{i}{4}a_1\delta n_{epw},\\
(\partial_t + \nu_{01} + V_{01}\partial_x)a_{01} &= -\frac{i\omega_{00}}{4\omega_1}a_1\delta n_{iaw},\\
(\partial_t + \nu_1 + V_1\partial_x)a_1 &= -\frac{i\omega_{00}}{4\omega_1}\left(\delta n^*_{epw}a_{00} + \delta n^*_{iaw}a_{01}\right),\\
(\partial_t + \nu_2 + V_2\partial_x)\delta n_{epw} &= -\frac{4i\Gamma^2_{\mathrm{SRS}}\omega_1 c^2}{\omega^3_{00}v^2_{00}}a_{00}a^*_1,\\
\left(\partial^2_t + V^2_3\partial^2_x\right)\delta n_{iaw} &= -\frac{Z\beta n_e(x)k^2_{iaw}c^2}{2n_c\omega^2_{00}}a_{01}a^*_1,
\end{aligned}
\tag{1}
$$

where a_{00}, a_{01}, and a_1 are slowly varying amplitudes of the SRS pump wave, the SC-SBS pump wave, and the seed wave, respectively. δn_{epw} and δn_{iaw} are the electron density perturbations of the Langmuir wave and the ion acoustic wave, respectively, which are normalized to n_c, where n_c is the critical density of the SRS pump laser. When a_{00} equals to 0, Eqs. (1) become the envelope coupling equations for Scheme 1.

In Scheme 2, SRS and SC-SBS share one seed laser; therefore, waves in Eq. (1) should satisfy the phase-matching conditions:

$$
\begin{aligned}
\omega_{00} &= \omega_1 + \omega_{epw},\\
\omega_{01} &= \omega_1 + \omega_{iaw},\\
|k_{epw}| &= |k_{00}| + |k_1|,\\
|k_{iaw}| &= |k_{01}| + |k_1|,
\end{aligned}
\tag{2}
$$

where ω_{00}, ω_{01}, ω_1, ω_{epw}, and ω_{iaw} are the frequency of five waves, and k_{00}, k_{01}, k_1, k_{epw}, and k_{iaw} are the corresponding wave numbers. In practice, ω_{01} is usually equals to ω_1, because $\omega_{iaw} \ll \omega_1$; thus, $|k_{iaw}| = 2|k_1|$. V_{00}, V_{01}, V_1, V_2, and V_3 are the group velocity of five waves. and $V_1 = -V_{01}$. ν_{00}, ν_{01}, ν_1, and ν_2 are the corresponding damping rates (for simplicity, the collision dampings of lasers are neglected), and ν_2 is the

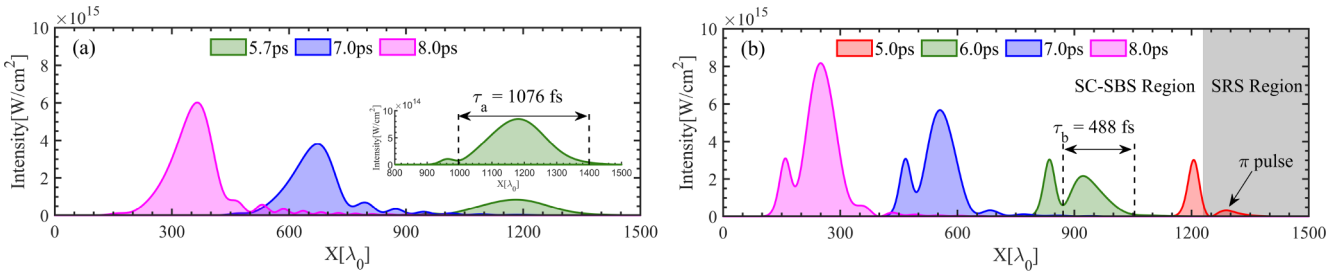

FIG. 2. Numerical solution of Eq. (1). (a) Amplification of Scheme 1. The inset figure is the seed laser at $t = 5.7$ ps. (b) Amplification of Scheme 2 with $L_{\rm SRS}/L_{\rm total} = 0.18$.

Landau damping of the Langmuir wave. Z is the charge state of ions, $\beta = m_e/m_i$ is the mass ratio of electrons and ions, and $n_e(x)$ is the plasma density.

As we know, weak-coupling SBS will transit to SC-SBS because of the higher intensity of the pump laser, and the threshold of SC-SBS has been studied in the early work [50],

$$(v_{01}/c)^2 > 4k_{01}V_3\omega_1 v_e^2/(\omega_{pe}c)^2, \tag{3}$$

where v_{01} is the electron oscillation velocity in the SC-SBS pump laser, ω_{pe} is the plasma frequency. The density perturbation of the ion acoustic wave oscillates rapidly over an acoustic period, and thus we retain the second derivative term in the equation of the ion acoustic wave. The maximum growth rate of SC-SBS is related to the amplitude of the pump laser,

$$\Gamma_{\text{SC-SBS}} = \frac{\sqrt{3}}{2}\left(\frac{k_{01}^2 v_{01}^2 \omega_{pi}^2}{2\omega_1}\right)^{1/3}, \tag{4}$$

where ω_{pi} is the plasma ion frequency. Besides, the growth rate of SRS in Scheme 2 is [44]

$$\Gamma_{\rm SRS} = \frac{k_{epw}v_{00}}{4}\left[\frac{\omega_{pe}^2}{\omega_{epw}(\omega_{00}-\omega_{epw})}\right]^{1/2}, \tag{5}$$

where v_{00} is the electron oscillation velocity in the SRS pump laser.

In Schemes 1 and 2, hydrogen plasma is used; i.e., $Z = 1$ and $m_i = 1836m_e$ for ions. The temperatures of electrons and ions are $T_e = 300$ eV and $T_i = 6$ eV, which gives $ZT_e/T_i = 50$. Compared with the plasma temperatures in recent works [35,51], the ion temperature in this paper is lower; we choose a lower ion temperature to reduce the influence of Landau damping [29]. The plasma density ranges from 0 to $0.04n_c$. The wavelengths of the SRS pump laser and the SC-SBS pump laser are $\lambda_0 = 800$ nm and $\lambda_{01} = 1000$ nm, respectively, and the wavelength of the seed laser also equals to 1000 nm. Both the intensities of the SRS pump laser and the SC-SBS pump laser are 4×10^{14} W/cm^2, and the intensity of the seed laser is 1×10^{14} W/cm^2. The initial seed laser has a Gaussian wave form with $\tau_{\rm FWHM} = 160$ fs. Under these conditions, SBS is in the strong-coupling regime for $n_e > 0.005n_c$ based on Eq. (3). The growth rates of SRS and SC-SBS are $\Gamma_{\rm SRS} = 0.0029\omega_{00}$ and $\Gamma_{\text{SC-SBS}} = 0.0011\omega_{00}$ when $n_e = 0.04n_c$, and the growth rate of SC-SBS decreases when the plasma density gets lower.

III. NUMERICAL SOLUTION OF THE FIVE-WAVE AMPLIFICATION MODEL

In order to investigate the difference between these two amplification schemes, Eq. (1) is numerically solved by the Lax-Wendroff method [52]. The total length of the simulation box is $L_{\rm total} = 1.2$ mm, and the space and time are discretized by $dx = 0.2c/\omega_{00}$ and $dt = 0.2\omega_{00}^{-1}$, respectively. The total simulation time is 8 ps, and the seed laser starts to enter the simulation box at around 4 ps. In Scheme 2 around 18% of plasma length is used for SRS amplification.

Figure 2(a) shows the amplification process by Scheme 1. In the linear stage, the pulse width of the seed laser increases, because the maximum of the seed laser moves with the half speed of light [1,18,31,32,34]. Since the initial pulse width of the seed laser is much smaller than that of the effective amplification width [18,32], $\tau_{\rm eff} = 1/\Gamma_{\rm SCSBS}$, the second pulse is formed and the intensity of the first peak still equals to 1×10^{14} W/cm^2, shown by the green area in Fig. 2(a). The duration of the SBS peak is $\tau_a = 1076$ fs (duration between two dashed lines) at $t = 5.7$ ps. The duration of the SBS peak reduces in the nonlinear stage, when the pump depletion happens [7,8]. At $t = 8.0$ ps, the duration of the SBS peak is 675 fs and the intensity of the seed laser increases to 6.02×10^{15} W/cm^2.

The results of Scheme 2 are shown in Fig. 2(b). At $t = 5.0$ ps, the seed laser has just entered the SC-SBS region, and it has been amplified to around 3.0×10^{15} W/cm^2 by SRS. The π pulse of SRS is also observed due to the pump depletion, and the intensity of the π pulse is 3.2×10^{14} W/cm^2. When pump depletion happens, the spatial derivative in the seed laser equation can be neglected, and then the equation reduces to a sine-Gordon equation. Malkin *et al.* found the particular solution of this equation is that the seed laser repeats itself as time, which is called self-similar solution or π-pulse solution [1,2].

We find that the structure of the seed laser after SRS amplification is similar to the green area in Fig. 2(a); the leading peak of the seed laser barely changes in the SC-SBS region, but the second peak is responsible for the amplification. We believe that the SBS peaks are seeded by the leading peak of SRS, because the SBS peak appears after the delay time it takes to develop.

Another finding in Fig. 2(b) is that the pulse duration is shorter, $\tau_b = 488$ fs (duration between two dashed lines), and the intensity of the seed laser grows faster

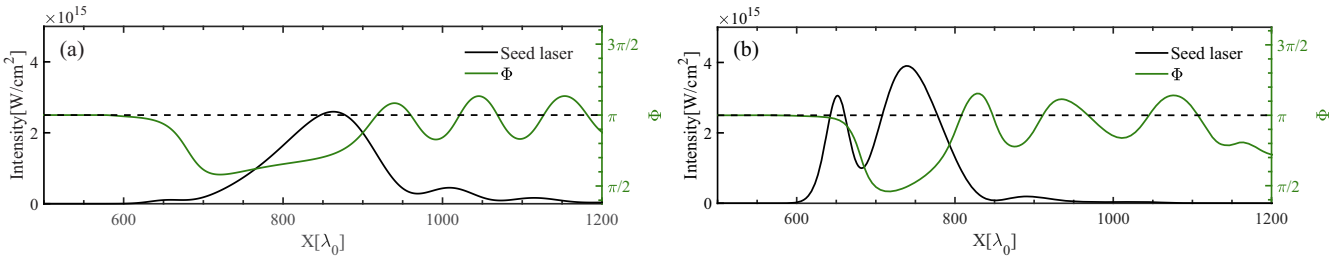

FIG. 3. Numerical solution of Eq. (1). (a) Results of Scheme 1. The black line is the seed laser at $t = 6.5$ ps, and the green line is the corresponding total phase in SC-SBS amplification. (b) Results of Scheme 2. The black line is the seed laser at $t = 6.5$ ps, and the green line is the corresponding total phase in SC-SBS amplification.

than in Scheme 1. At $t = 8.0$ ps, the seed laser is amplified to 8.17×10^{15} W/cm^2, which is 36% higher than the intensity in Fig. 2(a), and the duration of the SBS peak is 408 fs, which is shorter than that in Scheme 1. Next, we discuss reasons why these phenomena happen.

Chiaramello *et al*. studied the SC-SBS by the phase analysis of three waves [38,48]. We decide to follow their method by separating the amplitudes and phases of three waves in SC-SBS, the amplitude and phase equations can be written as

$$\begin{aligned}
(\partial_t + V_{01}\partial_x)|a_{01}| &= -\mu|a_1||\delta n_{iaw}|\sin(\Phi),\\
(\partial_t + V_{01}\partial_x)\varphi_{01} &= -\mu|\delta n_{iaw}|\frac{|a_1|}{|a_{01}|}\cos(\Phi),\\
(\partial_t + V_1\partial_x)|a_1| &= \mu|a_{01}||\delta n_{iaw}|\sin(\Phi),\\
(\partial_t + V_1\partial_x)\varphi_1 &= -\mu|\delta n_{iaw}|\frac{|a_{01}|}{|a_1|}\cos(\Phi),\\
\partial_t^2|\delta n_{iaw}| - |\delta n_{iaw}|(\partial_t\varphi)^2 - V_3^2\left[\partial_x^2|\delta n_{iaw}| - |\delta n_{iaw}|(\partial_x\varphi)^2\right] &= -\Lambda|a_{01}||a_1|\cos(\Phi),\\
|\delta n_{iaw}|\partial_t^2\varphi + 2\partial_t|\delta n_{iaw}|\partial_t\varphi - V_3^2\left(2\partial_x|\delta n_{iaw}|\partial_x\varphi + |\delta n_{iaw}|\partial_x^2\varphi\right) &= -\Lambda|a_{01}||a_1|\sin(\Phi),
\end{aligned} \tag{6}$$

where $\mu = \frac{\omega_{00}}{4\omega_1}$ and $\Lambda = \frac{Z\beta n_e(x)k_{iaw}^2c^2}{2n_c\omega_{00}^2}$. The amplitudes of three waves, $|a_{01}|$, $|a_1|$, and $|\delta n_{iaw}|$ in Eq. (6), are real and positive; φ_{01}, φ_1, and φ are corresponding phases; and Φ is the total phase, which is obtained by $\Phi = \mathrm{mod}(\varphi_{01} - \varphi_1 - \varphi, 2\pi)$.

From Eq. (6), we know that the energy flows from the pump laser to the seed laser when $\sin(\Phi) > 0$, leading to the seed laser growing in the exponential stage [38], while the energy flows from the seed laser to the pump laser when $\sin(\Phi) < 0$, which appears when the pump laser is depleted, and the π pulses appear.

The initial condition of phases are $\varphi_{01}(t_0) = 0$, $\varphi_1(t_0) = 0$, and $\varphi(t_0) = -\pi$, so $\Phi(t_0) = \pi$. At the early stage when the pump laser just collides with the seed laser, the phases of the pump laser and the ion acoustic wave keep constant, only φ_1 changes, and thus $\Phi(t) = \pi - \varphi_1(t)$. When the pump depletion occurs, the phase change of the pump laser should be considered, and the total phase Φ will change back to π. Once Φ becomes larger than π, the energy will flow from the seed laser back to the pump laser, and π pulses of the seed laser will appear. The length of the first interval of the total phase corresponds to the pulse width of the seed laser. In Fig. 3, we obtain the total phase of Schemes 1 and 2 at $t = 6.5$ ps. We observe that the width of the first interval in Scheme 2 is shorter than that in Scheme 1. Based on Amiranoff *et al.*'s work [38], the total phase changes faster when the initial intensity of the seed laser is higher, and the pulse width of seed laser is related to I_{s0}/I_p [38],

$$l_{\mathrm{interval}} = |V_1|\tau_{\mathrm{eff}}\frac{6}{I_{s0}/I_p + 5}, \tag{7}$$

where I_{s0} is the intensity of the seed laser when it enter into the SC-SBS region, and I_p is the intensity of the pump laser. In Scheme 2, $I_{s0}/I_p = 7.5$, so the pulse width in Scheme 2 is nearly half of that in Scheme 1.

We also obtain that the energy transfer efficiency, defined by $\eta = \int_0^{\tau_s} I_{\mathrm{seed}}(t)dt / \int_0^{t_{\mathrm{total}}} I_{\mathrm{pump}}(t)dt$, where τ_s is the duration of the seed laser at the end of simulation, for these two schemes in Fig. 2 are both around 70%. Therefore, it is easy to understand the higher intensity of the seed laser obtained in Scheme 2, since its pulse width in Scheme 2 is shorter. Another evidence is that, in Fig. 3(b), the minimum value of Φ in Scheme 2 is closer to $\pi/2$, or $\sin(\Phi)$ is closer to 1, which explains why the seed laser grows faster than that in Scheme 1.

Besides, we also observe that the slope of the second peak in Scheme 2 is steeper than that in Scheme 1. In the early work about SRS amplification, Tsidulko *et al*. found that the intensity and shape of the final amplified pulses are closely related to the local slope of the wave front of the seed laser [4]; the steeper the slope of the wave front is, the better the

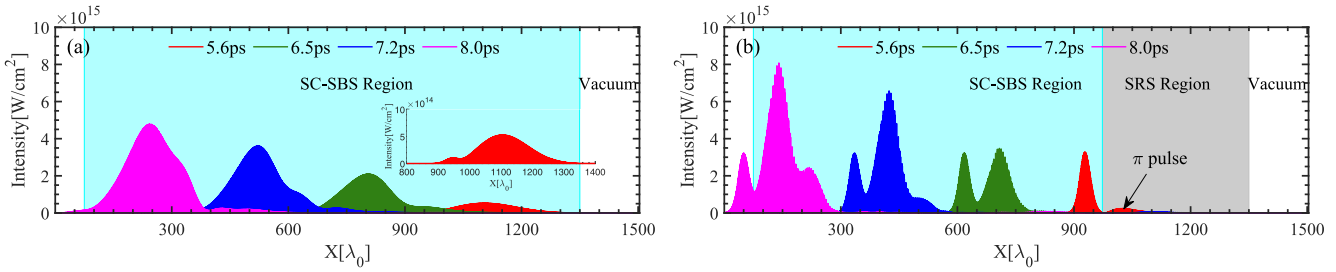

FIG. 4. VLAMA simulation results. (a) Amplification results of Scheme 1. The inset is the seed laser at $t = 5.6$ ps. (b) Amplification results of Scheme 2 with $L_{\mathrm{SRS}}/L_{\mathrm{total}} = 0.25$.

amplification will be. In the SRS region of Scheme 2, the slope of the seed front becomes steeper because of seed compression. In Fig. 2(b), the slope of the wave front of the SBS peak is nearly equal to that of first peak, i.e., the SRS peak. Thus, in Scheme 2 the SRS amplification not only improves the intensity but also steepens the seed front, which are both favorable to SC-SBS amplification.

We have considered changing the ordering of the pump pulses and adapting correspondingly, because the seed amplification is no better than that in Scheme 2. Under the plasma conditions and the laser conditions in this paper, Raman amplification first and then SC-SBS amplification is the better choice.

The precursor in Scheme 2 contains part of the energy, which is a disadvantage; however, when the SBS peak is seeded by the leading peak of SRS, the higher intensity of the precursor results in faster growth of the SBS peak. Thus, the precursor has a double-edged effect on SC-SBS amplification.

The envelope coupling model in Eq. (1) is a simplified model to analyze the SRS amplification and the SC-SBS amplification since it does not consider some nonlinear effects, such as harmonic waves, particle trapping, and nonlinear Landau damping. In the next two sections, we use fully kinetic simulation codes, Vlasov-Maxwell code (VLAMA) and PIC code (EPOCH), to verify the differences of these two schemes.

IV. ONE-DIMENSIONAL KINETIC VLASOV-MAXWELL SIMULATIONS

Plasma parameters in the VLAMA simulations are the same as those in Sec. III. Five percent vacuum space is reserved on the left of the simulation box and 10% vacuum space is reserved on the right; $L_{\mathrm{SRS}}/L_{\mathrm{total}} = 0.25$, where $L_{\mathrm{total}} = 1.2$ mm. The conditions for lasers are also the same as those in Sec. III. The space and time are discretized by $dx = 0.2c/\omega_0$ and $dt = 0.2\omega_0^{-1}$. The velocity space of electrons is $[-0.5c, 0.5c]$, and the velocity space of ions is $[-0.002c, 0.002c]$. The space-velocity mesh grid of electron and ion distribution functions are both 47232×2049.

Figure 4(a) is the amplification process by Scheme 1, similar to the results of five-wave simulations. At the linear stage, the duration of the seed laser is widened, and there are two peaks of the seed laser that have formed due to the initial seed duration shorter than $1/\Gamma_{(\mathrm{SC\text{-}SBS})}$ shown by the red line at $t = 5.6$ ps. Then, the duration of the seed laser has a little change at the nonlinear stage. After amplification, the maximum intensity of the seed laser becomes 4.8×10^{15} W/cm^2. Figure 4(b) shows the results of Scheme 2. After SRS amplification, the intensity of the leading peak becomes 3.3×10^{15} W/cm^2, and the π pulse of SRS is also observed. The intensity of the π pulse is 2.4×10^{14} W/cm^2. The leading peak of SRS will seed the SC-SBS amplification in the next stage. In the SC-SBS region, the intensity of the leading peak does not change and the second peak is amplified, which agrees with our five-wave simulations in Fig. 2. The pulse duration of the seed laser in Fig. 4(b) is shorter than that in Fig. 4(a), and the maximum intensity of our scheme is 8.12×10^{15} W/cm^2, which is much higher than that in Scheme 1. The time dependence of SBS peak intensities of two schemes are collected and shown in Fig. 5. The growth of the seed laser in Scheme 2 is faster than that in Scheme 1 in both the linear stage (exponential growth) and the nonlinear stage (linear growth). This is because of the length reduction of the first phase interval discussed in Sec. III.

Besides, by changing the ratio of the SRS length, i.e., $L_{\mathrm{SRS}}/L_{\mathrm{total}}$, we find that the SBS peak intensity increases first and then decreases with $L_{\mathrm{SRS}}/L_{\mathrm{total}}$ as shown by the black squares in Fig. 6. The maximum intensity of the SBS peak is 8.12×10^{15} W/cm^2 when $L_{\mathrm{SRS}}/L_{\mathrm{total}} = 0.25$. However, the SBS peak intensity decreases when $L_{\mathrm{SRS}}/L_{\mathrm{total}} > 0.25$, because the SC-SBS amplification length reduces with the increase of $L_{\mathrm{SRS}}/L_{\mathrm{total}}$, leading to the existence of the maximum SBS peak intensity in Fig. 6.

As shown by the green circles in Fig. 6, the energy transfer efficiency η in VLAMA simulations is also obtained. Normally, η in SC-SBS is higher than that in SRS [26,29], because based on Manley-Rowe relations the frequency of the ion acoustic wave is much less than the frequency of the pump

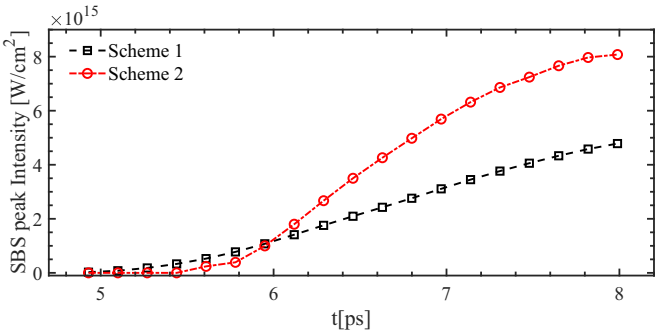

FIG. 5. Time dependence of SBS peak intensity in VLAMA simulations. The black squares stand for Scheme 1 and the red circles represent the results of Scheme 2.

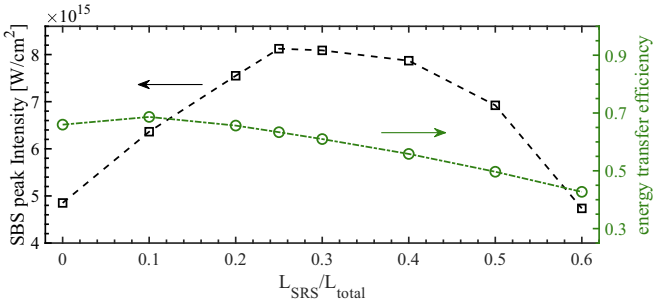

FIG. 6. Vlama simulation results. The black squares are the SBS peak intensities varying with $L_{\rm SRS}/L_{\rm total}$. The green circles are the energy transfer efficiency varying with $L_{\rm SRS}/L_{\rm total}$.

laser in SC-SBS, so the energy loss to the plasma wave is lower than in SRS. The energy transfer efficiency of the pure SC-SBS scheme is around 66%, and it decreases with $L_{\rm SRS}/L_{\rm total}$. We also observe that when $L_{\rm SRS}/L_{\rm total} = 0.25$, $\eta = 63\%$, which only decreases 3%, compared with Scheme 1. Thus, in Scheme 2 the maximum intensity of the SBS peak increases, but the energy transfer efficiency is not much lower than that of SC-SBS. The results of VLAMA simulations agree with those of the five-wave amplification model very well.

V. TWO-DIMENSIONAL PIC SIMULATIONS

In order to verify our proposed scheme in higher dimensions, we turn to use the two-dimensional and fully kinetic PIC simulation code EPOCH [53]. The plasma type and temperature are the same as those in the Vlasov simulations. The simulation box is $L_x = 0.8$ mm and $L_y = 128$ μm, and there are 30 cells per λ_0 at the longitudinal direction and 8 cells per λ_0 at the transverse direction. The intensities of the SBS pump laser and the SRS pump laser are both 4×10^{14} W/cm^2, and they are simple plane wave. The intensity of the seed laser is a Gaussian laser with an intensity of 1×10^{14} W/cm^2, FWHM = 160 fs, and a pulse width in the transverse dimension of 16 μm. Five percent vacuum space on both sides of the simulation box is maintained. In the pure SC-SBS amplification case, the plasma density ranges from 0 to $0.04n_c$, and there is 20% uniform density for SRS amplification in Scheme 2. For both electrons and ions, the particle number per cell is 100.

Figure 7(a) illustrates the results of 2D PIC simulations for Scheme 1. The duration of the seed laser is larger than that of Scheme 2 shown in Fig. 7(b). After interaction, the seed laser peak intensity is 1.74×10^{15} W/cm^2 and the maximum intensity in Scheme 2 is 4.28×10^{15} W/cm^2. The maximum intensity is more than double with the pure SC-SBS scheme. In Fig. 7(b), the first peak of the seed laser, i.e., the SRS peak, is clearly observed, and its intensity has little change through the SC-SBS amplification, which agrees well with the previous analyses. However, the filamentation of the seed laser is observed in Fig. 7(b). Filamentation effects are also observed in the early works [28,36,54], because of the ponderomotive effect, or the thermal effect, which makes the refractive index toward the center at the transverse direction. We obtain the theoretical growth rate of filamentation for the seed laser by $\gamma_{\rm filam} = 1/8(v_{\rm osc}/v_e)^2\omega_{pe}^2/\omega_0 = 0.025\omega_0$ (when the intensity of the seed laser is 4.0×10^{15} W/cm^2) [43]. In Fig. 7(b), the filamentation growth rate for simulation is $\gamma_{\rm filam} = 0.0242\omega_0$. Thus, the filamentation is mostly related to the high intensity of the seed laser. However, with the filamentation, Scheme 2 still has a better performance than Scheme 1. In future work, we will focus on the filamentation effects in Scheme 2.

VI. CONCLUSION AND DISCUSSION

In this paper, first, we propose a scheme to improve SC-SBS amplification with the assistance of SRS amplification, we construct a five-wave amplification model, and then we numerically solve the five-wave envelope equations to study the influence of SRS amplification on SC-SBS amplification. In comparison with pure SC-SBS amplification, our scheme increases the maximum intensity of the seed laser and reduces the pulse width of the seed laser, and the π pulse of SRS can seed the SC-SBS amplification. We find that the reason for this phenomenon is that (i) the width of the first interval of the total phase becomes shorter in our scheme because of the higher intensity of the seed laser when it enters the SC-SBS region and (ii) the energy transfer efficiency changes a little compared with the pure SC-SBS scheme. Next, the VLAMA simulations are carried out to test our schemes. The maximum intensity of the seed laser is improved nearly 69% in our scheme, the optimal $L_{\rm SRS}/L_{\rm total}$ ratio is tested as 0.25, and the energy transfer efficiency changes little when $L_{\rm SRS}/L_{\rm total} = 0.25$ compared with the pure SC-SBS amplification. At last, the two-dimensional PIC code is used to verify our conclusion, which qualitatively agrees with our predications.

As is well known, SC-SBS has higher energy transfer efficiency, but it also has a wider pulse width than that of SRS

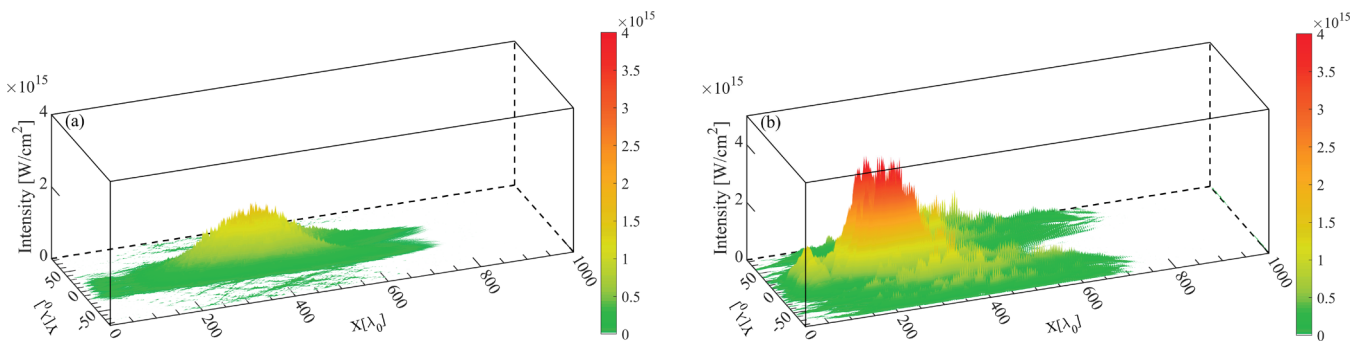

FIG. 7. 2D PIC simulation results. (a) Amplified seed laser in the pure SC-SBS scheme. (b) Amplified seed laser in our scheme.

[30,31,34,48,55]. Our scheme reduces the width of the first interval of the total phase, so the intensity of the seed laser is easier to increase at the nonlinear stage than in the pure SC-SBS scheme. The SC-SBS pump laser, the SRS pump laser, and the seed laser in our scheme are easy to get in experiments, because their wavelengths are close to the wavelengths of common laser devices. Besides, in experiments, the plasma profiles are usually Gaussian type [51], the plasma density change rate is small at the center, and it is possible to implement SRS amplification at this part of plasma. Our scheme does not require extra input energy from the pump laser; also the initial seed laser does not require additional processing.

ACKNOWLEDGMENTS

We are pleased to acknowledge useful discussions with Y. G. Chen, S. X. Xie, N. Peng, W. B. Yao, and S. Tan. This work was supported by the Scientific Research Foundation for High-level Talents of Anhui University of Science and Technology (Grant No. 2022yjrc106), the Natural Science Research Key Project of Anhui Educational Committee (Grant No. 2022AH050835) the Strategic Priority Research Program of Chinese Academy of Sciences (Grant No. XDA25050700), the National Natural Science Foundation of China (Grants No. 11805062, No. 11875091, and No. 11975059), the Science Challenge Project (Grant No. TZ2016005), and the Natural Science Foundation of Hunan Province, China (Grant No. 2020JJ5029).

[1] V. M. Malkin, G. Shvets, and N. J. Fisch, Phys. Rev. Lett. **82**, 4448 (1999).
[2] V. M. Malkin, G. Shvets, and N. J. Fisch, Phys. Rev. Lett. **84**, 1208 (2000).
[3] D. Strickland and G. Mourou, Opt. Commun. **55**, 447 (1985).
[4] Yu. A. Tsidulko, V. M. Malkin, and N. J. Fisch, Phys. Rev. Lett. **88**, 235004 (2002).
[5] G. M. Fraiman, N. A. Yampolsky, V. M. Malkin, and N. J. Fisch, Phys. Plasmas **9**, 3617 (2002).
[6] R. M. G. M. Trines, F. Fiúza, R. Bingham, R. A. Fonseca, L. O. Silva, R. A. Cairns, and P. A. Norreys, Nat. Phys. **7**, 87 (2011).
[7] J. Ren, W. Cheng, S. Li, and S. Suckewer, Nat. Phys. **3**, 732 (2007).
[8] Z. Toroker, V. M. Malkin, and N. J. Fisch, Phys. Rev. Lett. **109**, 085003 (2012).
[9] B. Ersfeld and D. A. Jaroszynski, Phys. Rev. Lett. **95**, 165002 (2005).
[10] R. Nuter and V. Tikhonchuk, Phys. Rev. E **87**, 043109 (2013).
[11] K. Qu, I. Barth, and N. J. Fisch, Phys. Rev. Lett. **118**, 164801 (2017).
[12] I. Barth and N. J. Fisch, Phys. Rev. E **97**, 033201 (2018).
[13] M. R. Edwards, Y. Shi, J. M. Mikhailova, and N. J. Fisch, Phys. Rev. Lett. **123**, 025001 (2019).
[14] M. R. Edwards, K. Qu, J. M. Mikhailova, and N. J. Fisch, Phys. Plasmas **24**, 103110 (2017).
[15] Z. Wu, Q. Chen, A. Morozov, and S. Suckewer, Phys. Plasmas **26**, 103111 (2019).
[16] D. Haberberger, A. Davies, J. L. Shaw, R. K. Follett, J. P. Palastro, and D. H. Froula, Phys. Plasmas **28**, 062311 (2021).
[17] Y. G. Chen, Y. Chen, S. X. Xie, N. Peng, J. Q. Yu, and C. Z. Xiao, Chin. Phys. B **30**, 105202 (2021).
[18] G. Lehmann, K. H. Spatschek, and G. Sewell, Phys. Rev. E **87**, 063107 (2013).
[19] Y. Ping, W. Cheng, S. Suckewer, D. S. Clark, and N. J. Fisch, Phys. Rev. Lett. **92**, 175007 (2004).
[20] C.-H. Pai, M.-W. Lin, L.-C. Ha, S.-T. Huang, Y.-C. Tsou, H.-H. Chu, J.-Y. Lin, J. Wang, and S.-Y. Chen, Phys. Rev. Lett. **101**, 065005 (2008).
[21] Z. Toroker, V. M. Malkin, and N. J. Fisch, Phys. Plasmas **21**, 113110 (2014).
[22] R. M. G. M. Trines, F. Fiúza, R. Bingham, R. A. Fonseca, L. O. Silva, R. A. Cairns, and P. A. Norreys, Phys. Rev. Lett. **107**, 105002 (2011).
[23] A. A. Solodov, V. M. Malkin, and N. J. Fisch, Phys. Plasmas **10**, 2540 (2003).
[24] C. Riconda, S. Weber, L. Lancia, J.-R. Marquès, G. Mourou, and J. Fuchs, Plasma Phys. Controlled Fusion **57**, 014002 (2015).
[25] M. R. Edwards, N. J. Fisch, and J. M. Mikhailova, Phys. Rev. Lett. **116**, 015004 (2016).
[26] M. R. Edwards, Q. Jia, J. M. Mikhailova, and N. J. Fisch, Phys. Plasmas **23**, 083122 (2016).
[27] Y. Chen, C. Y. Zheng, Z. J. Liu, L. H. Cao, Q. S. Feng, and C. Z. Xiao, Plasma Phys. Controlled Fusion **62**, 105020 (2020).
[28] S. Weber, C. Riconda, L. Lancia, J.-R. Marquès, G. A. Mourou, and J. Fuchs, Phys. Rev. Lett. **111**, 055004 (2013).
[29] A. A. Andreev, C. Riconda, V. T. Tikhonchuk, and S. Weber, Phys. Plasmas **13**, 053110 (2006).
[30] L. Lancia, J.-R. Marquès, M. Nakatsutsumi, C. Riconda, S. Weber, S. Hüller, A. Mančić, P. Antici, V. T. Tikhonchuk, A. Héron, P. Audebert, and J. Fuchs, Phys. Rev. Lett. **104**, 025001 (2010).
[31] F. Schluck, G. Lehmann, C. Müller, and K. H. Spatschek, Phys. Plasmas **23**, 083105 (2016).
[32] F. Schluck, G. Lehmann, and K. H. Spatschek, Phys. Plasmas **22**, 093104 (2015)()
[33] Q. Jia, I. Barth, M. R. Edwards, J. M. Mikhailova, and N. J. Fisch, Phys. Plasmas **23**, 053118 (2016).
[34] G. Lehmann and K. H. Spatschek, Phys. Plasmas **20**, 073112 (2013).
[35] M. Chiaramello, C. Riconda, F. Amiranoff, J. Fuchs, M. Grech, L. Lancia, J.-R. Marquès, T. Vinci, and S. Weber, Phys. Plasmas **23**, 072103 (2016).
[36] E. P. Alves, R. M. G. M. Trines, K. A. Humphrey, R. Bingham, R. A. Cairns, F. Fiúza, R. A. Fonseca, and L. O. Silva, Plasma Phys. Controlled Fusion **63**, 114004 (2021).
[37] K. A. Humphrey, R. M. G. M. Trines, F. Fiuza, D. C. Speirs, P. Norreys, R. A. Cairns, L. O. Silva, and R. Bingham, Phys. Plasmas **20**, 102114 (2013).

[38] F. Amiranoff, C. Riconda, M. Chiaramello, L. Lancia, J. R. Marquès, and S. Weber, Phys. Plasmas **25**, 013114 (2018).
[39] C. Riconda, S. Weber, L. Lancia, J.-R. Marquès, G. A. Mourou, and J. Fuchs, Phys. Plasmas **20**, 083115 (2013).
[40] G. Lehmann and K. H. Spatschek, Phys. Plasmas **22**, 043105 (2015).
[41] G. Lehmann and K. H. Spatschek, Phys. Plasmas **23**, 023107 (2016).
[42] M. Shoucri, J.-P. Matte, and F. Vidal, Phys. Plasmas **22**, 053101 (2015).
[43] W. L. Kruer, *The Physics of Laser Plasma Interactions* (Westview, Boulder, CO, 2003).
[44] D. R. Nicholson, *Introduction to Plasma Theory* (Wiley & Sons, New York, 1983).
[45] V. M. Malkin and N. J. Fisch, Phys. Plasmas **8**, 4698 (2001).
[46] Z. Toroker, V. M. Malkin, A. A. Balakin, G. M. Fraiman, and N. J. Fisch, Phys. Plasmas **19**, 083110 (2012).
[47] D. Turnbull, S. Bucht, A. Davies, D. Haberberger, T. Kessler, J. L. Shaw, and D. H. Froula, Phys. Rev. Lett. **120**, 024801 (2018).
[48] M. Chiaramello, F. Amiranoff, C. Riconda, and S. Weber, Phys. Rev. Lett. **117**, 235003 (2016).
[49] Z. J. Liu, S. P. Zhu, L. H. Cao, and C. Y. Zheng, Acta Phys. Sin. (Overseas Ed.) **56**, 7084 (2007).
[50] D. W. Forslund, J. M. Kindel, and E. L. Lindman, Phys. Fluids **18**, 1002 (1975).
[51] L. Lancia, A. Giribono, L. Vassura, M. Chiaramello, C. Riconda, S. Weber, A. Castan, A. Chatelain, A. Frank, T. Gangolf, M. N. Quinn, J. Fuchs, and J.-R. Marquès, Phys. Rev. Lett. **116**, 075001 (2016).
[52] Y. Chen, C. Y. Zheng, Z. J. Liu, L. H. Cao, Q. S. Feng, Y. G. Chen, Z. M. Huang, and C. Z. Xiao, Plasma Phys. Controlled Fusion **63**, 055004 (2021).
[53] T. D. Arber, K. Bennett, C. S. Brady, A. Lawrence-Douglas, M. G. Ramsay, N. J. Sircombe, P. Gillies, R. G. Evans, H. Schmitz, A. R. Bell, and C. P. Ridgers, Plasma Phys. Controlled Fusion **57**, 113001 (2015).
[54] L. L. Zhao, Y. L. Zuo, J. Q. Su, and S. H. Yang, Phys. Plasmas **26**, 093102 (2019).
[55] R. M. G. M. Trines, E. P. Alves, E. Webb, J. Vieira, F. Fiúza, R. A. Fonseca, L. O. Silva, R. A. Cairns, and R. Bingham, Sci. Rep. **10**, 19875 (2020).